analytical chemistry

Article

pubs.acs.org/ac

Integration of Quartz Crystal Microbalance-Dissipation and Reflection-Mode Localized Surface Plasmon Resonance Sensors for Biomacromolecular Interaction Analysis

Abdul Rahim Ferhan,[†] Joshua A. Jackman,[†] and Nam-Joon Cho*[,†,‡]

[†]School of Materials Science and Engineering, Nanyang Technological University, 50 Nanyang Avenue, Singapore 639798

[‡]School of Chemical and Biomedical Engineering, Nanyang Technological University, 62 Nanyang Drive, Singapore 637459

Supporting Information

ABSTRACT: The combination of label-free, surface-sensitive measurement techniques based on different physical principles enables detailed characterization of biomacromolecular interactions at solid−liquid interfaces. To date, most combined measurement systems have involved experimental techniques with similar probing volumes, whereas the potential of utilizing techniques with different surface sensitivities remains largely unexplored, especially for data interpretation. Herein, we report a combined measurement approach that integrates a conventional quartz crystal microbalance-dissipation (QCM-D) setup with a reflection-mode localized surface plasmon (LSPR) sensor. Using this platform, we investigate vesicle adsorption on a titanium oxide-coated sensing substrate along with the amphipathic, α-helical (AH) peptide-induced structural transformation of surface-adsorbed lipid vesicles into a supported lipid bilayer (SLB) as a model biomacromolecular interaction. While the QCM-D and LSPR signals both detected mass uptake arising from vesicle adsorption, tracking the AH peptide-induced structural transformation revealed more complex measurement responses based on the different surface sensitivities of the two techniques. In particular, the LSPR signal recorded an increase in optical mass near the sensor surface which indicated SLB formation, whereas the QCM-D signals detected a significant loss in net acoustic mass due to excess lipid and coupled solvent leaving the probing volume. Importantly, these measurement capabilities allowed us to temporally distinguish the process of SLB formation at the sensor surface from the overall structural transformation process. Looking forward, these label-free measurement capabilities to simultaneously probe adsorbates at multiple length scales will provide new insights into complex biomacromolecular interactions.

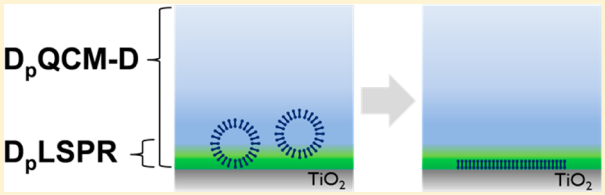

In biological systems, macromolecular assemblies undergo dynamic interaction processes at interfaces, and clarifying the mechanistic details of these processes is important for a wide range of fundamental and applied research fields.[1−6] Among relevant topics of interest, the adsorption behavior of macromolecular assemblies at solid−liquid interfaces is particularly interesting and has motivated the development of highly surface-sensitive, label-free measurement techniques in order to track a wide range of biomacromolecular interaction processes, including substrate-mediated vesicle fusion as well as protein−lipid and protein−protein interactions.[7−10] Optical biosensors such as surface plasmon resonance (SPR),[11−13] ellipsometry,[14−16] and reflectometry[17,18] enable detailed quantification of the total number of biomolecules within the probing volume, with decay lengths typically extending up to hundreds of nanometers from the sensor surface and high sensitivity to the optical properties of biomolecules.[12,19] On the other hand, acoustic biosensors such as the quartz crystal microbalance-dissipation (QCM-D) technique are utilized in order to characterize the conformational properties of adsorbed biomolecules,[20−24] and QCM-D in particular is widely employed because it is sensitive to the mass and viscoelastic properties of adsorbed biomolecules and hydrodynamically coupled solvent mass. For conventional QCM-D instruments, the penetration depth is in the range of 60 to 250 nm,[25] which is compatible with the typical range of optical biosensors. For this reason, there is significant interest in exploring the integration of optical and acoustic biosensors into combined experimental configurations that enable simultaneous measurements of biomacromolecular processes occurring at the same interface in real-time.

Toward this goal, there have been extensive efforts aimed at coupling QCM-D measurements with SPR,[26−28] ellipsometry,[29,30] and reflectometry[31−33] in order to characterize processes such as vesicle adsorption, protein binding, and amphipathic, α-helical (AH) peptide-mediated rupture of adsorbed lipid vesicles. One key advantage of combined measurement approaches is that several independent physical parameters can be measured simultaneously, thereby enabling a more detailed understanding of complex biological processes.[34] For example, combined QCM-D and reflectometry measurements have revealed that AH peptide-induced rupture of adsorbed lipid vesicles is a multistage process that involves

Received: November 2, 2016
Accepted: November 25, 2016
Published: November 25, 2016

DOI: 10.1021/acs.analchem.6b04303
Anal. Chem. 2016, 88, 12524−12531

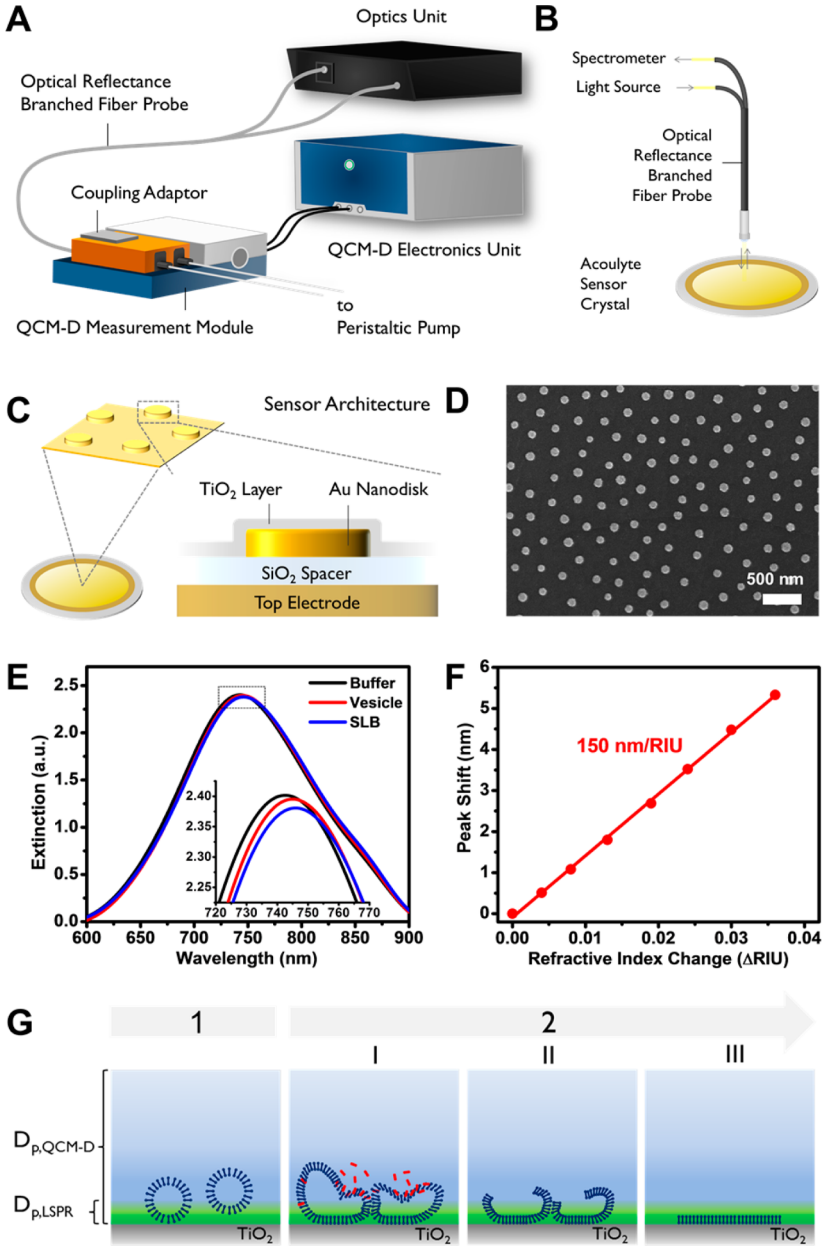

Figure 1. (A) Overview of the combined QCM-D and LSPR instrument setup. (B) Simplified description of the LSPR sensing configuration. (C) Architecture of sensing surface, which is a modified QCM-D sensor chip and the top electrode is coated with a SiO_2 spacer layer on top of which a nanodisk array is present. (D) SEM micrograph of the titanium oxide-coated sensor. (E) LSPR extinction spectra obtained after the introduction of buffer (black trace), after the adsorption of intact vesicles (red trace), and after SLB formation (blue trace). The region bound by the rectangular box is enlarged in the inset to highlight the peak shift after each step. (F) LSPR peak shift as a function of bulk refractive index change (ΔRIU) in glycerol/water mixtures. (G) Illustration of biomacromolecular events involving (1) vesicle adsorption and (2) AH peptide-mediated SLB formation. The relative penetration depths (D_p) of the QCM-D and LSPR signals are shown.

peptide binding to the vesicle bilayer followed by vesicle swelling and membrane morphological responses leading to vesicle rupture and supported lipid bilayer (SLB) formation.[31] In such embodiments, the probing volume of the two measurement techniques is comparable, and hence, the parameters being tracked by each technique reflect the physical properties of the same adsorbate layer. Therefore, calculated values such as the optical mass (biomolecular mass only) and the acoustic mass (biomolecular and coupled solvent mass) can be compared in order to determine the hydration fraction of the adsorbate.

While combined measurement approaches with comparable probing volumes have merits for direct comparison of adlayer properties, alternative sensing configurations are also possible, whereby the optical and acoustic biosensors have mismatched probing volumes that can be advantageous for studying biomolecular interactions. In particular, highly surface-sensitive, optical-based nanoplasmonic sensors with decay lengths on the order of 5−20 nm have been paired with QCM-D sensors in order to investigate biomolecular adsorption processes. Dahlin et al. reported synchronized nanoplasmonic and QCM-D sensing experiments and highlighted the advantages of interpreting measurement data collected simultaneously by

DOI: 10.1021/acs.analchem.6b04303
Anal. Chem. 2016, 88, 12524−12531

both measurement techniques in order to reveal otherwise undetectable structural changes (e.g., conformational change in polymers from extended to confined state) in adlayer properties.[35] Jonsson et al. also conducted simultaneous nanoplasmonic and QCM-D sensing experiments in order to investigate vesicle adsorption and rupture on silica-coated surfaces as well as quantification of subsequent protein binding.[36] In addition, Larsson et al. reported combined LSPR and QCM-D measurements on silica-coated nanodisk arrays in order to also investigate vesicle adsorption and rupture to form SLBs as well as protein binding.[37] In these past studies, significant emphasis was placed on sensor and instrumentation development, primarily driven by the need to design QCM-D sensing modules that facilitate simultaneous optical transmission measurements. Indeed, the previous works involved specialized QCM-D measurement setups (i.e., electrodeless configurations or electrode modification). While the existing studies successfully demonstrate the merits of simultaneous nanoplasmonic and QCM-D measurements, conventional QCM-D measurement platforms do not facilitate simultaneous optical measurements in transmission mode. Therefore, the development of an integrated measurement setup that permits simultaneous LSPR and QCM-D measurements in a conventional measurement platform would be advantageous.

Herein, we report a combined measurement setup that integrates a reflection-mode LSPR sensor with a conventional QCM-D instrument platform. Using this platform, we investigate vesicle adsorption on a titanium oxide-coated sensing substrate along with the AH peptide-induced structural transformation of surface-adsorbed lipid vesicles into an SLB as a model biomacromolecular interaction. One key advantage of studying this vesicle-to-bilayer structural transformation is that the surface sensitivities of the two measurement techniques are well-positioned to spatially isolate the processes of vesicle rupture and SLB formation. In the previous combined nanoplasmonic and QCM-D sensor works, the decay length of the nanoplasmonic evanescent field was mainly discussed from the perspective of its quantification, with limited attention to the variation in probing volume of the two techniques. Recently, LSPR has been mainly discussed as an alternative to other optical biosensors because it has simpler technical requirements. In this work, we extend discussion of these merits by further demonstrating how combined QCM-D and LSPR sensing strategies can be utilized to gain new insights into biomacromolecular systems based on mismatched probing volumes, which in turn enable simultaneous tracking of structural transformations occurring at different length scales from the sensor surface.

EXPERIMENTAL SECTION

Measurement Setup. The combined QCM-D and LSPR setup is composed of the Q-Sense E1 system with Q-Sense QWM401 window module (Biolin Scientific, Stockholm, Sweden) together with the Insplorion Acoulyte module (Insplorion AB, Gothenburg, Sweden), which provides an optical connection between the QCM-D measurement chamber and the Insplorion X-Nano optics unit (Insplorion AB, Gothenburg, Sweden). Measurements were performed on the Acoulyte quartz crystal sensor, which is a modified version of a regular Q-Sense quartz crystal sensor upon which randomly distributed, titanium oxide-coated gold nanodisks are fabricated.

Data Analysis. QCM-D data analysis was performed using the Voigt–Voinova model[38] available on the Q-Tools software package (Biolin Scientific). The LSPR data analysis was performed with the Insplorer software package (Insplorion AB). The spectral resolution of the plasmon resonance was determined by high-order polynomial fitting, and the centroid position, which is denoted as the LSPR peak position in this work, was calculated from the fit.[39] More detailed information can be found in the Supporting Information.

RESULTS AND DISCUSSION

Sensor Design. The combined QCM-D and LSPR sensing approach is based on a conventional QCM-D instrument (Q-Sense E1) that is coupled to a commercial LSPR instrument (Insplorion XNano) via an integrated sensor module (Insplorion Acoulyte) that is compatible with a branched fiber optics reflectance probe (Figure 1A). The probe end of the fiber is fitted over the window module, which is secured onto the QCM-D measurement chamber and houses the sensor while each of the branched ends is connected to the spectrometer and light source, respectively, both of which are contained within the Insplorion optics unit. The reflectance probe serves as a two-way optical connection between the optics unit and the measurement chamber (Figure 1B). An advantage of conducting optical measurements in reflection mode is that it allows conventional QCM-D crystals to be used with minimal modification. The sensor chip used in this study is a standard gold-coated QCM-D crystal, upon which a 100 nm thick layer of silicon dioxide was coated on the top electrode by plasma-enhanced chemical vapor deposition. An array of well-separated gold nanodisk optical transducers was fabricated on top of this coating by hole-mask colloidal lithography, followed by a thin (~10 nm) conformal layer of titanium dioxide across the sensing substrate, which was achieved by atomic layer deposition (Figure 1C). An SEM image of the gold nanodisk array is presented in Figure 1D, demonstrating the large separation distance between neighboring nanodisks, which are ~100 nm and ~20 nm in diameter and height, respectively.

The interaction of light with the gold nanodisks leads to the resonant oscillation of conduction electrons resulting in maximum light extinction at the resonant wavelength, which is known as the extinction peak (λ_{max}), around 745 nm for our system (Figure 1E). Refractive index changes in the vicinity of the gold nanodisks cause shifts in λ_{max}, herein referred as the LSPR peak shift, allowing the characterization of molecular mass changes close to the surface and providing a spectral signature for adsorbed biomolecules such as vesicles or an SLB. As the LSPR measurements are conducted in reflection mode, light passes through the nanoplasmonic sensing layer twice before reaching the spectrometer, resulting in higher peak extinction and higher detection sensitivity.[40−42] We also characterized the bulk refractive index sensitivity of the nanoplasmonic sensors as the measurement sensitivity can vary depending on the nanoparticle fabrication process each time. Using a titration series of glycerol–water mixtures (0–35 wt % glycerol), $\Delta\lambda_{max}$ measurements identified that the sensors have a bulk refractive index sensitivity of 150 nm/RIU (Figure 1F). This value agrees well with previously reported titanium-oxide-coated gold nanodisk sensor arrays which were operated in transmission mode.[43] In parallel to the LSPR measurements, QCM-D measurements are simultaneously conducted on the same sensor surface and track mass and viscoelastic properties of the adlayer properties by monitoring changes in resonance

DOI: 10.1021/acs.analchem.6b04303
Anal. Chem. 2016, 88, 12524–12531

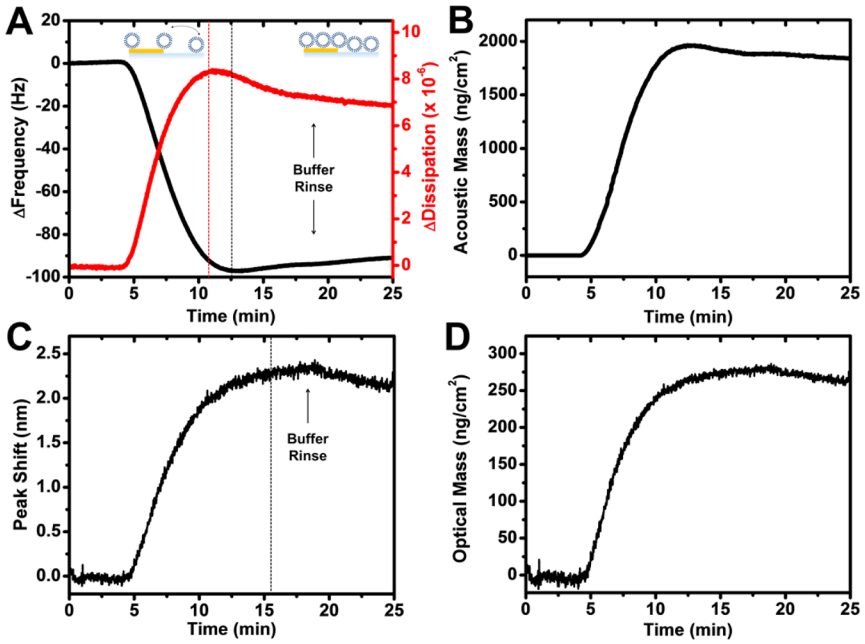

Figure 2. (A) QCM-D frequency and dissipation shifts as a function of time for vesicle adsorption onto titanium oxide. The vertical lines are included as a guide to the different time points when minimum frequency and maximum dissipation shifts are observed during the overshoots. (B) Effective acoustic mass as a function of time based on the QCM-D measurement data in panel (A), as determined by Voigt–Voinova modeling. (C) LSPR peak shift as a function of time for vesicle adsorption onto titanium oxide, which was simultaneously recorded on the same substrate in parallel to the QCM-D measurement data reported in panel (A). The vertical line indicates the time when stabilization is reached. (D) Optical mass as a function of time, which is extracted from the LSPR peak shift data in panel (C) based on the Lorenz–Lorentz relation [see eqs (1)–(3) in the Supporting Information].

frequency (4.95 MHz fundamental frequency) and energy dissipation, respectively.

On the basis of this measurement configuration, we proceeded to investigate two different biomacromolecular events (Figure 1G). The first event is monotonic adsorption of zwitterionic lipid vesicles onto the titanium oxide-coated surface. It is known that zwitterionic lipid vesicles adsorb onto titanium oxide and remain intact, forming a saturated layer of intact vesicles on the surface.[23,44,45] The second event involves addition of AH peptide to the adsorbed vesicle layer, which promotes vesicle rupture and a resulting structural transformation from adsorbed vesicles to an SLB.[46−48] As both of these events have been extensively studied in standalone QCM-D or LSPR measurement configurations along with other combined systems as described above, they provide useful model systems to investigate the analytical merits of the present system.

Vesicle Adsorption onto Titanium Oxide. We first monitored lipid vesicle adsorption onto the titanium oxide-coated sensor substrate. After establishing a baseline signal in aqueous buffer solution, 0.5 mg/mL zwitterionic 67 nm diameter 1,2-dioleoyl-*sn*-glycero-3-phosphocholine (DOPC) lipid vesicles were added, leading to a decrease in resonance frequency and an increase in energy dissipation starting from t = 5 min (Figure 2A). The final frequency and energy dissipation shifts were −90 Hz and 6.8 × 10^{-6}, respectively, which are indicative of a saturated adlayer of small vesicles.[49] As adsorbed vesicles form a soft, viscoelastic adlayer, the Voigt–Voinova model was applied in order to estimate the acoustic mass (lipid and coupled solvent), which plateaued around 1950 ng/cm^2 (Figure 2B).

One interesting observation was that both QCM-D measurement signals exhibited overshoot behavior with maximum responses around t = 11 to 13 min—a feature, which is not conventionally seen for vesicle adsorption on flat titanium oxide substrates[50] and is likely attributed to the influence of the nanostructure geometry.[51] Typically, such behavior is observed when adsorbed vesicles in the medium surface coverage regime are weakly attached (e.g., on the edges of nanodisks) and therefore exhibit "rocking and rolling" motion which increases the energy dissipation of the adsorbate.[52] As more vesicles become adsorbed around the nanodisks, the packing arrangement becomes tighter, leading to greater ordering and a decrease in the energy dissipation.

This observation is corroborated by simultaneous LSPR measurement which indicates monotonic vesicle adsorption, yielding a $\Delta\lambda_{max}$ shift of 2.3 nm, which agrees well with past transmission-mode LSPR measurements[53−55] (Figure 2C). As the LSPR signal is sensitive to the lipid mass only, the result supports that the overshoot behavior observed in the QCM-D measurement arises from complex hydrodynamic responses associated with coupled solvent rather than loss of lipid mass. Another important observation is that overshooting of the QCM-D frequency and dissipation shifts occur 2 to 3 min before the LSPR signal stabilizes. Hence, interpretation of the combined measurement results supports that the overshoot responses occur in the medium-coverage regime of adsorbed vesicles, and the QCM-D signals approach stabilization around the same time as the LSPR signal. Taking into account the known refractive index of adsorbed vesicles, we also computed the optical mass measured by the LSPR technique, and the optical mass value (lipid only) reached ∼275 ng/cm^2 at saturation (Figure 2D). As expected, this value is appreciably lower than previous values (∼1000 ng/cm^2) estimated by reflectometry and ellipsometry measurements[29,31] because the LSPR technique is more highly surface-sensitive and captures

DOI: 10.1021/acs.analchem.6b04303
Anal. Chem. 2016, 88, 12524−12531

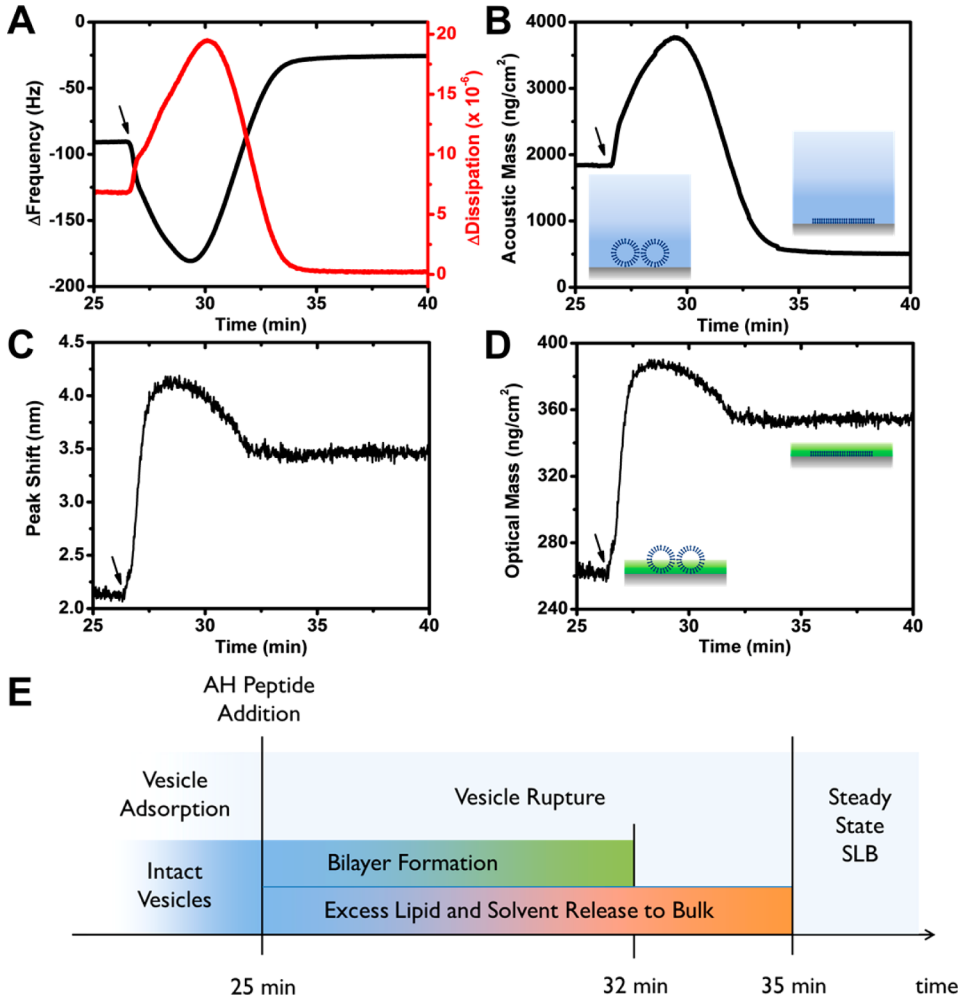

Figure 3. (A) QCM-D frequency and dissipation shifts as a function of time for AH peptide-mediated structural transformation of adsorbed vesicles into SLB. AH peptide was added at t = 27 min. (B) Temporal variation in the acoustic mass as determined by analysis of the QCM-D measurement data. (C) Corresponding peak shift as a function of time. (D) Temporal variation in the optical mass as determined by analysis of the LSPR measurement data. (E) Chronology of events highlighting vesicle rupture, SLB formation, and release of excess lipid occurring over different time scales.

only a fraction of the total lipid mass which is near the sensor surface.

AH Peptide-Mediated Structural Transformation. We next monitored AH peptide-mediated vesicle rupture and tracked the resulting structural transformation from adsorbed vesicles into an SLB. After vesicle adsorption reached saturation and there were stable measurement values, 13 μM AH peptide was added resulting in a gradual decrease in frequency from −80 to −180 Hz due to vesicle swelling prior to rupture.[31] After reaching this inflection point, the frequency increased before finally stabilizing at −25 Hz, which is indicative of an SLB. In parallel, there was an increase in the energy dissipation signal from 7.5 × 10^{-6} up to 20 × 10^{-6}, before returning to nearly zero (Figure 3A). As such, the final values of the QCM-D frequency and dissipation shifts confirm the successful formation of an SLB on titanium oxide. As the QCM-D measurement technique has a relatively large probing volume, it should be emphasized that the measurement responses indicate a *net loss* of acoustic mass during the vesicle-to-bilayer structural transformation. The acoustic mass values estimated by the Voigt−Voinova model further support this measurement result, and it is consistent with excess lipid from ruptured vesicles leaving the sensor surface upon SLB formation (Figure 3B).

Accordingly, the LSPR peak shift also increased sharply upon initial AH peptide addition before a slight decrease and eventual stabilization (Figure 3C). The final $\Delta\lambda_{max}$ shift was 3.5 nm, whereas a saturated layer of adsorbed vesicles yielded a $\Delta\lambda_{max}$ shift of only 2.3 nm. As LSPR is a highly surface-sensitive technique, this finding indicates that the measurement responses of the reflection-mode LSPR sensor agree well with those from previous transmission-mode systems.[56] When vesicle adsorption occurs onto a surface, the packing arrangement reaches a jamming limit (estimated to be around 0.58 to 0.70), and hence, the surface cannot be completely covered by adsorbed vesicles.[50,53] Upon SLB formation, the sensor surface, including the nanodisks, becomes coated with a lipid bilayer, and the result is that the lipid mass is, on average, nearer to the sensor surface.

Hence, while the total lipid mass in the adsorbed layer decreases, there is a *net increase* of optical mass during the vesicle-to-bilayer structural transformation, as monitored by the LSPR technique (Figure 3D). This finding underscores the high surface sensitivity of the LSPR measurement approach because previous combined systems involving simultaneous QCM-D and reflectometry or ellipsometry always showed *net decreases in both acoustic and optical mass.*[29−31] In these previous

DOI: 10.1021/acs.analchem.6b04303
Anal. Chem. 2016, 88, 12524−12531

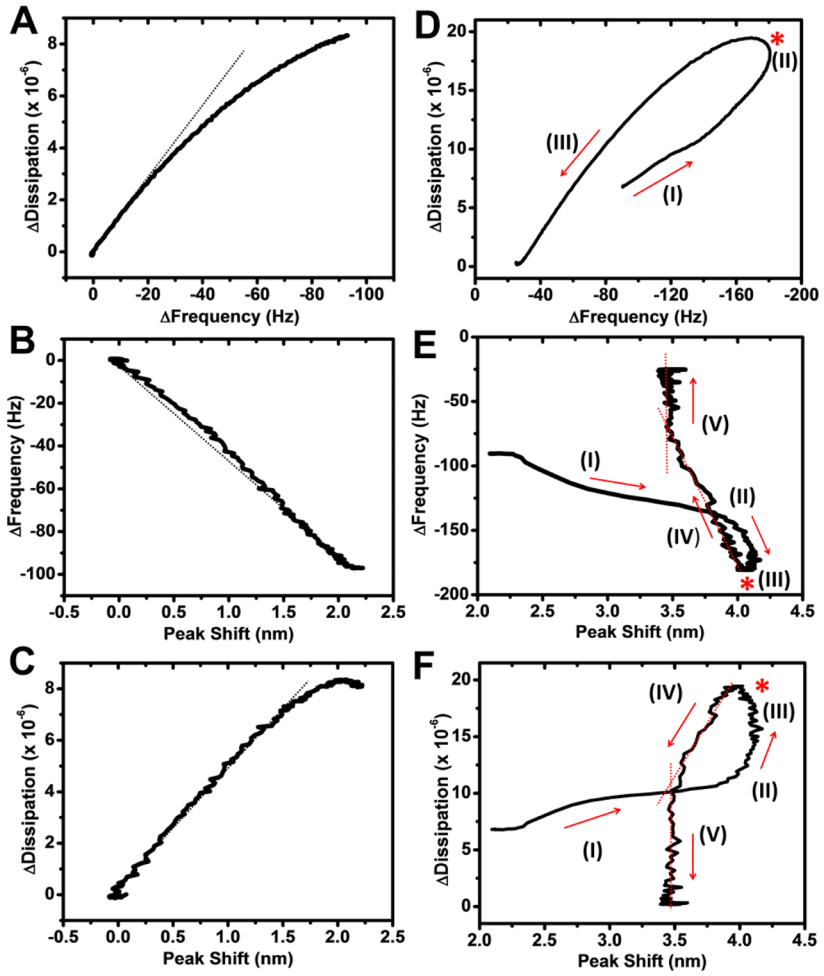

Figure 4. Time-independent curves correlating changes in (A) resonance frequency to energy dissipation, (B) peak shift to frequency shift, and (C) peak shift to energy dissipation, observed during vesicle adsorption onto titanium oxide. Time-independent curves correlating changes in (D) resonance frequency to energy dissipation, (E) peak shift to frequency shift, and (F) peak shift to energy dissipation, observed during the AH peptide-mediated vesicle-to-bilayer structural transformation.

demonstrations, AH peptide-mediated vesicle rupture induced SLB formation which led to an overall decrease in both the acoustic and optical masses. As mentioned above, the difference in these measurement responses is attributed to the varying surface sensitivities of the different optical techniques because LSPR has a much smaller probing volume than reflectometry and ellipsometry, as well as other plasmonic measurement approaches (see, e.g., ref 57). To our knowledge, this result is the first example of a biomacromolecular interaction event in which simultaneously measured acoustic and optical responses show opposite mass changes in the adlayer mass properties.

As the QCM-D and LSPR measurement techniques are sensitive to different regions within the adlayer, we also identified that the corresponding interaction kinetics are sensitive to different aspects of the AH peptide-induced vesicle-to-bilayer structural transformation. Indeed, it was observed that the LSPR signal stabilized first, indicating that SLB formation occurs before excess lipid is removed from the QCM-D probing volume (Figure 3E).

Comparison of QCM-D and LSPR Measurement Signals. In this section, we compare the QCM-D and LSPR measurement signals in order to evaluate the biomacromolecular interactions in more detail.

Vesicle Adsorption. We first analyzed the time-independent curve describing the relationship between the QCM-D frequency and dissipation (f–D) signals, which is frequently used to describe the viscoelastic contribution of the adsorbing species.[58] During intact vesicle adsorption, a correlation between frequency and dissipation was observed, with near linearity in the low surface coverage regime (Figure 4A). At higher surface coverages, the deviation from linearity is attributed to the adlayer becoming more rigid when close packing of adsorbed vesicles is achieved. Extending this analysis to the combined measurement results, we also plotted the time-independent curve describing the relationship between the QCM-D frequency versus LSPR peak shifts (λ–f). A linear correlation was observed between the decrease in frequency and increase in peak shift, indicating that both signals exhibit a nearly direct correspondence with the number of adsorbed vesicles for the small vesicles in this case (Figure 4B).

In addition, the time-independent curve of the QCM-D energy dissipation versus LSPR peak shift signals (λ–D) showed more complex behavior. During the adsorption of intact vesicles, the dissipation shift increased linearly as the peak shift reached 1.5 nm, before deviating with further increase in peak shift from 1.5 to 2.3 nm (Figure 4C). As such, this deviation occurred when the adsorbed mass increased to ~66%

DOI: 10.1021/acs.analchem.6b04303
Anal. Chem. 2016, 88, 12524−12531

of the total optical mass at saturation, indicating that further vesicle adsorption to higher surface coverages does not contribute additional viscoelastic character to the adlayer properties. This finding is particularly important because it is often reported that the QCM-D frequency shift is not proportional to the number of adsorbed particles, and the QCM-D energy dissipation shift is regarded as a better indicator of surface coverage.[50] As seen here, the evidence supports that the QCM-D energy dissipation signal cannot capture differences in the vesicle packing at high surface coverages, while the LSPR signal is more sensitive to vesicle adsorption at high coverages.

AH Peptide-Mediated Structural Transformation. We next investigated the AH peptide-mediated SLB formation process, and the $f-D$ curve indicates that the structural transformation can be broken down into three steps (Figure 4D).

In step (I), a decrease in frequency accompanied by an increase in dissipation indicates vesicle swelling, until turning point (II) when vesicles rupture and the frequency increases gradually. In the final step (III), the dissipation eventually decreased following a further increase in frequency resulting from the loss of lipid and solvent.

By comparison, the combination of QCM-D and LSPR measurement responses reveals deeper insight into the structural transformation. Figure 4E shows that the process can be broken down into five steps based on the $\lambda-f$ curve. In step (I), a gradual decrease in frequency accompanied by a sharp increase in peak shift indicates significant accumulation of optical mass on the surface compared to the overall increase in acoustic mass. This stage is followed by step (II), which is characterized by a continued sharp drop in frequency while the peak shift stabilizes, indicating the saturation of optical mass on the surface as the total acoustic mass continues to increase because of vesicle swelling and resulting morphological changes that increase the amount of coupled solvent. Hence, a significant extent of peptide binding is necessary before gross morphological changes occur as part of the vesicle swelling process. Once vesicle rupture becomes the predominant event recorded in the ensemble-average measurements, there is a sharp turning point (III), leading to steps (IV) and (V). In step (IV), a gradual decrease in peak shift is accompanied by a sharp increase in frequency, implying that lipid reorganization and SLB formation involves a relatively small decrease in optical mass, which is removed from the surface amidst a much larger decrease in acoustic mass arising from the vesicle-to-bilayer structural transformation and concomitant loss of coupled solvent. Importantly, in the final step (V), it is observed that the frequency continues to increase despite no further LSPR peak shift. This step indicates that the completion of SLB formation at the sensor surface precedes the complete removal of excess lipid from the probing volume.

In addition, the $\lambda-D$ curve also reveals a five-step process for the AH peptide-mediated structural transformation (Figure 4F). The first step is an (I) increase in peak shift with minimal increase in dissipation corresponding to AH peptide binding. This is followed by an (II) abrupt, 2-fold increase in dissipation as the peak shift stabilizes, reflecting primarily vesicle swelling and associated increases in coupled solvent. The vesicle rupture process is manifested in the prominent inflection point (III) as the dissipation begins to drop sharply with minimal change of the peak shift in step (IV), and there is no further peak shift in the final step (V). Combining the observation from the $\lambda-f$ curve, we note that, after vesicle rupture, there is only minor contribution from lipid loss to the drop in dissipation. Overall, this approach emphasizes the advantage of combining techniques with different penetration depths, which enables processes that occur at different surface proximities to be clearly distinguished with high temporal resolution.

CONCLUSIONS

In summary, we have demonstrated the measurement capabilities of a combined experimental approach that integrates a quartz crystal microbalance-dissipation (QCM-D) sensor with a reflection-mode localized surface plasmon (LSPR) sensor. This approach is the first demonstration of a combined QCM-D and LSPR measurement system that is compatible with a conventional QCM-D instrument. By utilizing the different surface sensitivities of the QCM-D and LSPR measurement signals, our findings highlight the potential of deciphering complex biomacromolecular interactions, as exemplified by the model system involving AH peptide-mediated structural transformation of adsorbed vesicles into an SLB. Importantly, these capabilities enabled us to temporally distinguish the process of SLB formation at the sensor surface, which occurs before the structural transformation is complete. By taking advantage of simultaneous measurements that utilize surface-sensitive techniques with different probing volumes, there is excellent potential for improving our understanding of biomacromolecular interactions at solid–liquid interfaces. Aside from probing shape transformations, the integration of QCM-D and reflection-mode LSPR provides a versatile tool for studying other dynamic processes in biomacromolecular thin films as well, including temperature-dependent phase transitions, for example. Furthermore, from an analytical perspective, the measurement platform can be further expanded to include additional sensing elements such as highly sensitive reflective infrared spectroscopic techniques, thereby providing the potential capability to simultaneously perform detailed chemical analyses of the biomacromolecular interactions under investigation.

ASSOCIATED CONTENT

Supporting Information

The Supporting Information is available free of charge on the ACS Publications website at DOI: 10.1021/acs.analchem.6b04303.

Additional details for experimental protocols and data analysis (PDF)

AUTHOR INFORMATION

Corresponding Author

*E-mail: njcho@ntu.edu.sg (N.J.C.).

ORCID

Nam-Joon Cho: 0000-0002-8692-8955

Notes

The authors declare no competing financial interest.

ACKNOWLEDGMENTS

This work was supported by a National Research Foundation Proof-of-Concept Grant (NRF2015NRF-POC001-019).

REFERENCES

(1) Heinz, H.; Ramezani-Dakhel, H. *Chem. Soc. Rev.* **2016**, *45*, 412–448.

DOI: 10.1021/acs.analchem.6b04303
Anal. Chem. 2016, 88, 12524–12531

(2) Ariga, K. *ChemNanoMat* **2016**, *2*, 333−343.
(3) Watanabe, S.; Watarai, H. *Bull. Chem. Soc. Jpn.* **2015**, *88*, 955−962.
(4) Sheiko, S. S.; Zhou, J.; Arnold, J.; Neugebauer, D.; Matyjaszewski, K.; Tsitsilianis, C.; Tsukruk, V. V.; Carrillo, J.-M. Y.; Dobrynin, A. V.; Rubinstein, M. *Nat. Mater.* **2013**, *12*, 735−740.
(5) Mendes, P. M. *Chem. Soc. Rev.* **2013**, *42*, 9207−9218.
(6) Nel, A. E.; Madler, L.; Velegol, D.; Xia, T.; Hoek, E. M. V.; Somasundaran, P.; Klaessig, F.; Castranova, V.; Thompson, M. *Nat. Mater.* **2009**, *8*, 543−557.
(7) Ozkumur, E.; Needham, J. W.; Bergstein, D. A.; Gonzalez, R.; Cabodi, M.; Gershoni, J. M.; Goldberg, B. B.; Unlu, M. S. *Proc. Natl. Acad. Sci. U. S. A.* **2008**, *105*, 7988−7992.
(8) Citartan, M.; Gopinath, S. C. B.; Tominaga, J.; Tang, T.-H. *Analyst* **2013**, *138*, 3576−3592.
(9) Fan, X.; White, I. M.; Shopova, S. I.; Zhu, H.; Suter, J. D.; Sun, Y. *Anal. Chim. Acta* **2008**, *620*, 8−26.
(10) Hunt, H. K.; Armani, A. M. *Nanoscale* **2010**, *2*, 1544−1559.
(11) Nguyen, H.; Park, J.; Kang, S.; Kim, M. *Sensors* **2015**, *15*, 10481.
(12) Homola, J. *Chem. Rev.* **2008**, *108*, 462−493.
(13) Homola, J.; Yee, S. S.; Gauglitz, G. *Sens. Actuators, B* **1999**, *54*, 3−15.
(14) Arwin, H. *Thin Solid Films* **2011**, *519*, 2589−2592.
(15) Losurdo, M. *Thin Solid Films* **2011**, *519*, 2575−2583.
(16) Elwing, H. *Biomaterials* **1998**, *19*, 397−406.
(17) Dijt, J. C.; Stuart, M. A. C.; Fleer, G. J. *Adv. Colloid Interface Sci.* **1994**, *50*, 79−101.
(18) Liu, X.; Dedinaite, A.; Nylander, T.; Dabkowska, A. P.; Skoda, M.; Makuska, R.; Claesson, P. M. *J. Colloid Interface Sci.* **2015**, *440*, 245−252.
(19) Horváth, R.; Lindvold, L. R.; Larsen, N. B. *Appl. Phys. B: Lasers Opt.* **2002**, *74*, 383−393.
(20) Höök, F.; Kasemo, B.; Nylander, T.; Fant, C.; Sott, K.; Elwing, H. *Anal. Chem.* **2001**, *73*, 5796−5804.
(21) Cho, N.-J.; Frank, C. W.; Kasemo, B.; Höök, F. *Nat. Protoc.* **2010**, *5*, 1096−1106.
(22) Keller, C. A.; Kasemo, B. *Biophys. J.* **1998**, *75*, 1397−1402.
(23) Reimhult, E.; Höök, F.; Kasemo, B. *J. Chem. Phys.* **2002**, *117*, 7401−7404.
(24) Ouberai, M. M.; Xu, K.; Welland, M. E. *Biomaterials* **2014**, *35*, 6157−6163.
(25) Keiji Kanazawa, K.; Gordon, J. G. *Anal. Chim. Acta* **1985**, *175*, 99−105.
(26) Kristensen, S. H.; Pedersen, G. A.; Nejsum, L. N.; Sutherland, D. S. *J. Phys. Chem. B* **2013**, *117*, 10376−10383.
(27) Reimhult, E.; Larsson, C.; Kasemo, B.; Höök, F. *Anal. Chem.* **2004**, *76*, 7211−7220.
(28) Reimhult, E.; Zäch, M.; Höök, F.; Kasemo, B. *Langmuir* **2006**, *22*, 3313−3319.
(29) Zan, G. H.; Cho, N.-J. *Colloids Surf., B* **2014**, *121*, 340−346.
(30) Zan, G. H.; Jackman, J. A.; Cho, N.-J. *J. Phys. Chem. B* **2014**, *118*, 3616−3621.
(31) Cho, N.-J.; Wang, G.; Edvardsson, M.; Glenn, J. S.; Hook, F.; Frank, C. W. *Anal. Chem.* **2009**, *81*, 4752−4761.
(32) Edvardsson, M.; Svedhem, S.; Wang, G.; Richter, R.; Rodahl, M.; Kasemo, B. *Anal. Chem.* **2009**, *81*, 349−361.
(33) Wang, G.; Rodahl, M.; Edvardsson, M.; Svedhem, S.; Ohlsson, G.; Höök, F.; Kasemo, B. *Rev. Sci. Instrum.* **2008**, *79*, 075107.
(34) Konradi, R.; Textor, M.; Reimhult, E. *Biosensors* **2012**, *2*, 341.
(35) Dahlin, A. B.; Jönsson, P.; Jonsson, M. P.; Schmid, E.; Zhou, Y.; Höök, F. *ACS Nano* **2008**, *2*, 2174−2182.
(36) Jonsson, M. P.; Jönsson, P.; Höök, F. *Anal. Chem.* **2008**, *80*, 7988−7995.
(37) Larsson, E. M.; Edvardsson, M. E. M.; Langhammer, C.; Zorić, I.; Kasemo, B. *Rev. Sci. Instrum.* **2009**, *80*, 125105.
(38) Cho, N.-J.; Kanazawa, K. K.; Glenn, J. S.; Frank, C. W. *Anal. Chem.* **2007**, *79*, 7027−7035.
(39) Dahlin, A. B.; Tegenfeldt, J. O.; Höök, F. *Anal. Chem.* **2006**, *78*, 4416−4423.
(40) Anker, J. N.; Hall, W. P.; Lyandres, O.; Shah, N. C.; Zhao, J.; Van Duyne, R. P. *Nat. Mater.* **2008**, *7*, 442−453.
(41) Endo, T.; Kerman, K.; Nagatani, N.; Hiepa, H. M.; Kim, D. K.; Yonezawa, Y.; Nakano, K.; Tamiya, E. *Anal. Chem.* **2006**, *78*, 6465−6475.
(42) Kedem, O.; Vaskevich, A.; Rubinstein, I. *J. Phys. Chem. C* **2014**, *118*, 8227−8244.
(43) Jackman, J. A.; Kim, M. C.; Zhdanov, V. P.; Cho, N.-J. *Phys. Chem. Chem. Phys.* **2016**, *18*, 3065−3072.
(44) Cho, N.-J.; Frank, C. W. *Langmuir* **2010**, *26*, 15706−15710.
(45) Jackman, J. A.; Zan, G. H.; Zhao, Z.; Cho, N.-J. *Langmuir* **2014**, *30*, 5368−5372.
(46) Cho, N.-J.; Cho, S.-J.; Cheong, K. H.; Glenn, J. S.; Frank, C. W. *J. Am. Chem. Soc.* **2007**, *129*, 10050−10051.
(47) Jackman, J. A.; Zan, G. H.; Zhdanov, V. P.; Cho, N.-J. *J. Phys. Chem. B* **2013**, *117*, 16117−16128.
(48) Jackman, J. A.; Goh, H. Z.; Zhdanov, V. P.; Knoll, W.; Cho, N.-J. *J. Am. Chem. Soc.* **2016**, *138*, 1406−1413.
(49) Reimhult, E.; Höök, F.; Kasemo, B. *Langmuir* **2003**, *19*, 1681−1691.
(50) Reviakine, I.; Rossetti, F. F.; Morozov, A. N.; Textor, M. *J. Chem. Phys.* **2005**, *122*, 204711.
(51) Malmström, J.; Agheli, H.; Kingshott, P.; Sutherland, D. S. *Langmuir* **2007**, *23*, 9760−9768.
(52) Reviakine, I.; Gallego, M.; Johannsmann, D.; Tellechea, E. *J. Chem. Phys.* **2012**, *136*, 084702.
(53) Jackman, J. A.; Zhdanov, V. P.; Cho, N.-J. *Langmuir* **2014**, *30*, 9494−9503.
(54) Oh, E.; Jackman, J. A.; Yorulmaz, S.; Zhdanov, V. P.; Lee, H.; Cho, N.-J. *Langmuir* **2015**, *31*, 771−781.
(55) Jackman, J. A.; Špačková, B.; Linardy, E.; Kim, M. C.; Yoon, B. K.; Homola, J.; Cho, N.-J. *Chem. Commun.* **2016**, *52*, 76−79.
(56) Zan, G. H.; Jackman, J. A.; Kim, S.-O.; Cho, N.-J. *Small* **2014**, *10*, 4828−4832.
(57) Jackman, J. A.; Linardy, E.; Yoo, D.; Seo, J.; Ng, W. B.; Klemme, D. J.; Wittenberg, N. J.; Oh, S. H.; Cho, N. J. *Small* **2016**, *12*, 1159.
(58) Keller, C.; Glasmästar, K.; Zhdanov, V.; Kasemo, B. *Phys. Rev. Lett.* **2000**, *84*, 5443.

DOI: 10.1021/acs.analchem.6b04303
Anal. Chem. 2016, 88, 12524−12531